Computer simulation of ionic transport in silver iodide within carbon nanotubes

Article *in* Solid State Ionics · April 2011

DOI: 10.1016/j.ssi.2010.11.020

5 authors, including:

Igor Yu. Gotlib
Saint Petersburg State University
27 PUBLICATIONS **87** CITATIONS
SEE PROFILE

A.K. Ivanov-Schitz
Moscow State Institute of International Relations
48 PUBLICATIONS **404** CITATIONS
SEE PROFILE

I.V. Murin
Saint Petersburg State University
218 PUBLICATIONS **1,358** CITATIONS
SEE PROFILE

Andrey Vitalievich Petrov
Saint Petersburg State University
80 PUBLICATIONS **490** CITATIONS
SEE PROFILE

Solid State Ionics 188 (2011) 6–14

Contents lists available at ScienceDirect

Solid State Ionics

journal homepage: www.elsevier.com/locate/ssi

Computer simulation of ionic transport in silver iodide within carbon nanotubes

I. Yu. Gotlib [a,*], A.K. Ivanov-Schitz [b], I.V. Murin [a], A.V. Petrov [a], R.M. Zakalyukin [b]

[a] Chemistry Department of Saint Petersburg State University, Universitetsky pr. 26, Petrodvorets, 198504 Saint Petersburg, Russia
[b] A. V. Shubnikov RAS Institute of Crystallography, Leninsky pr. 59, 119333 Moscow, Russia

ARTICLE INFO

Article history:
Received 1 June 2010
Received in revised form 9 November 2010
Accepted 13 November 2010
Available online 14 December 2010

Keywords:
Silver iodide
Carbon nanotubes
Inorganic nanotubes
Ionic transport

ABSTRACT

Filling of carbon single-wall nanotubes (SWNTs), of diameter $d = 11.5–15$ Å, by silver iodide from the melt is modeled by molecular dynamics. Formation of AgI inorganic nanotube (INT) structures in the SWNTs on cooling, and ion diffusion in AgI within the tubes (AgI@SWNT) at 500–1200 K are studied. Dependence of AgI@SWNT structure on carbon SWNT geometry is examined. For $d \leq 14.2$ Å, a single-wall AgI INT is formed within the carbon tube, with structure (geometry) depending on d; in wider tubes, there are extra silver and iodine ions in the central region. The calculated diffusion coefficients of silver and iodine ions and their diffusion activation energies depend on the nanotube geometry. Ion mobilities within carbon SWNTs are significantly lower, and diffusion activation energies, higher than in the bulk phase of AgI, especially in narrow tubes. In the (11,11) carbon SWNT, the widest among those simulated, the activation energy for silver ion diffusion becomes close to the "bulk" value, while for iodine ions, larger in size, the difference remains.

1. Introduction

In the last years, considerable attention has been directed to nanostructures of different compounds that can be formed within carbon nanotubes. Many molten inorganic substances including metal halides, oxides, etc. can be inserted into carbon single-wall nanotubes (SWNTs) and form specific crystalline structures there. In SWNTs with low diameter (in some cases, even ≤ 10 Å), single-wall inorganic nanotubes (INTs) are often formed. The inorganic nanostructures in carbon nanotubes have been studied both experimentally (HRTEM, Raman spectroscopy) and by computer simulation [1–9]; the structures often tend to be stable even at temperatures above the melting point of the bulk inorganic phase [10]. Geometry and physical properties of INTs formed by a given filler substance within a carbon SWNT depend on the SWNT geometry.

In nanostructured state of solid electrolytes, ion transport characteristics, as well as other properties, can be varied depending on structure and surrounding environment. Silver iodide is a well-known exemplary solid electrolyte. High-conducting α-AgI is thermodynamically stable in the temperature range from 420 K to the melting point at 828 K at low pressures. In this phase, I ions form a body-centered cubic lattice, whereas highly mobile Ag ions are randomly distributed through the equivalent interstices. At lower temperatures, β-modification (with a wurtzite-like hexagonal structure) becomes stable. A metastable γ-phase also exists below 420 K, having a zinc blende (sphalerite) structure. At pressures higher than 3000 atm, both α and β polymorphs undergo a transition to fcc-AgI (with a rocksalt-like structure) that is also an ionic conductor with high Ag ion mobility [11,12]. Some composites formed by AgI and insulating inorganic oxides (Al_2O_3, SiO_2 etc.) show still more enhanced conductivity [13].

Numerous computer simulation studies of bulk silver iodide and AgI-based systems (in solid and/or molten state) were reviewed in [14]. More publications appeared recently [15–17]. Isolated AgI nanoclusters were also simulated [18]; unlike in the cases of AgCl and AgBr, the lowest energy clusters of silver iodide were found to be polyhedral shells (including nanotubes, sphalerite fragments and hexagonal stacks), not "bulk crystal" fragments, most likely due to the same difference in ionic radii that makes the wurtzite structure of the bulk AgI preferable to the rocksalt one at low pressures.

In this work, we present a computer simulation study of AgI nanostructures that are formed within different carbon SWNTs with diameter $d < 15$ Å (AgI@SWNT structures). Available publications on the subject include some preliminary simulation results that describe filling thin carbon SWNTs with AgI [19]. Molecular dynamics (MD) simulations of model INT structures in [7] may also reproduce qualitatively some characteristics of AgI@SWNT, so far as the model potential used in that work was chosen to conform with basic structural characteristics of pure bulk AgI (preference for a hexagonal structure at low pressures and temperatures, with a transition to a rocksalt-like cubic phase at high pressures). Thermal stability and reactivity of composites consisting of AgCl, AgBr, or AgI encapsulated in carbon SWNTs were studied experimentally, using thermogravimetric analysis and Raman spectroscopy [20]. However, as far as we know, no detailed study has been reported of different AgI@SWNT structures that are formed in carbon nanotubes of different geometry.

* Corresponding author.
E-mail address: gotlib@ns.nonel.pu.ru (I.Y. Gotlib).

0167-2738/$ – see front matter © 2010 Elsevier B.V. All rights reserved.
doi:10.1016/j.ssi.2010.11.020

2. Model and simulation procedure

At the preliminary stage of the work, the bulk phase of AgI has been simulated. Then, filling of carbon SWNTs' by AgI from the melt has been modeled. The filling process can be simulated directly only for relatively short carbon tubes (25–40 Å in length); to reproduce AgI@SWNT structures in a long tube (~200 Å), several copies of AgI configuration, formed in a shorter tube, have been placed in the long SWNT and equilibrated. After that, the AgI@SWNT structures produced are analyzed, and ion mobility characteristics at different temperatures are determined.

To describe interactions in AgI, the standard Parrinello–Rahman–Vashishta model potential is used:

$$U_{ij} = \frac{q_i q_j}{r_{ij}} + \frac{H_{ij}}{r_{ij}^{n_{ij}}} - \frac{P_{ij}}{r_{ij}^4} - \frac{W_{ij}}{r_{ij}^6} \tag{1}$$

where r_{ij} is the distance between ions i and j; q_i, q_j are their effective charges; the parameters H_{ij}, n_{ij} describe short-range repulsion, W_{ij}, is van der Waals attraction, and P_{ij}, is polarization interactions: $P_{ij} = \frac{1}{2}\left(\alpha_i q_j^2 + \alpha_j q_i^2\right)$, α_i, α_j are the polarizabilities of ions i and j. This approximation was used, successfully enough, in computer modeling of AgI and other silver halide systems, starting from the original work by Parrinello, Rahman, and Vashishta [21]. (There are more sophisticated approximations, like the model used in [17], that are not pair-additive and include direct calculation of polarization interaction energy.)

At the first stage (simulations of the bulk AgI), two sets of parameters of potential (1) have been tested: the original Parrinello–Rahman–Vashishta (PRV) set [21] and the modified set proposed by Shimojo and Kobayashi (ShK) [22]. According to [22], the PRV parameters, when used in a MD simulation, give α-AgI bulk density lower than the experimental value (at 495 K, 5.474 g/cm^3 and 5.99 g/cm^3 respectively). The parameter values are given in Table 1.

Interactions between silver or iodine ions and carbon atoms are represented by Lennard–Jones potential:

$$U_{ij} = 4\varepsilon_{ij}\left(\left(\frac{\sigma_{ij}}{r_{ij}}\right)^{12} - \left(\frac{\sigma_{ij}}{r_{ij}}\right)^{6}\right). \tag{2}$$

The values of parameters are the same as in [19]: $\varepsilon_{IC} = 0.00683$ eV, $\sigma_{IC} = 3.736$ Å, $\varepsilon_{AgC} = 0.0335$ eV, $\sigma_{AgC} = 2.926$ Å.

To calculate interaction energy of carbon atoms in a nanotube, the Tersoff model potential [23] is used:

$$U_{ij} = f_C\left(r_{ij}\right)\left[f_R\left(r_{ij}\right) + b_{ij} f_A\left(r_{ij}\right)\right]; \tag{3a}$$

$$f_R\left(r_{ij}\right) = A_{ij}\exp\left(-\lambda_{ij} r_{ij}\right), \quad f_A\left(r_{ij}\right) = -B_{ij}\exp\left(-\mu_{ij} r_{ij}\right); \tag{3b}$$

$$f_C\left(r_{ij}\right) = \begin{cases} 1, r_{ij} \le R_{ij} \\ \frac{1}{2} + \frac{1}{2}\cos\frac{\pi\left(r_{ij} - R_{ij}\right)}{\left(S_{ij} - R_{ij}\right)}, R_{ij} < r_{ij} < S_{ij}; \\ 0, r_{ij} \ge S_{ij} \end{cases} \tag{3c}$$

$$\begin{aligned} &b_{ij} = \chi_{ij}\left(1 + \beta_i^{n_i}\zeta_{ij}^{n_i}\right)^{-1/2n_i}, \quad \zeta_{ij} = \sum_{k \ne i,j} f_C(r_{ik})\omega_{ik} g\left(\theta_{ijk}\right), \\ &\chi_{ii} = 1,\ \omega_{ii} = 1,\ \chi_{ij} = \chi_{ji},\ \omega_{ij} = \omega_{ji}, \\ &g\left(\theta_{ijk}\right) = 1 + \frac{c_i^2}{d_i^2} - \frac{c_i^2}{d_i^2 + \left(h_i - \cos\theta_{ijk}\right)^2}; \end{aligned} \tag{3d}$$

$$\begin{aligned} &\lambda_{ij} = \frac{\lambda_i + \lambda_j}{2},\ \mu_{ij} = \frac{\mu_i + \mu_j}{2},\ A_{ij} = \left(A_i A_j\right)^{1/2},\ B_{ij} = \left(B_i B_j\right)^{1/2}, \\ &R_{ij} = \left(R_i R_j\right)^{1/2},\ S_{ij} = \left(S_i S_j\right)^{1/2}. \end{aligned} \tag{3e}$$

Here, r_{ij} is the distance between atoms i and j, θ_{ijk} is the angle between i–j and i–k bonds. The parameter values for carbon are: $A_C = 1393.6$ eV; $B_C = 346.7$ eV; $\lambda_C = 3.4879$ Å^{-1}; $\mu_C = 2.2119$ Å^{-1}; $\beta_C = 1.5724 \cdot 10^{-7}$; $n_C = 0.72751$; $c_C = 3.8049 \cdot 10^4$; $d_C = 4.3484$; $h_C = -0.57058$; $R_C = 1.8$ Å; $S_C = 2.1$ Å.

To eliminate undesirable movement of a carbon nanotube as a whole and its large-scale deformation (bending or splitting), four C atoms at each of its ends are "frozen" in fixed positions, and in long tubes (200 Å), four C atoms close to the tube midpoint are also "frozen". The "containing sphere" potential is also imposed on the system when periodic boundary conditions are not used, to prevent AgI escape at high temperatures. The restraints on nanotube movement and deformation introduced in the simulations can be considered as approximating the behavior of nanotubes in tight bundles (that are quite common in experimental studies, and in reality can be held together not only by van der Waals cohesion but also by covalent bonding between neighboring carbon tubes).

Spherical cutoff is applied to van der Waals energy, at 24 Å, and to Coulomb energy, at 100 Å (except MD runs with periodic boundary conditions imposed on the system, when Ewald summation is used).

The DL_POLY software [24] has been used in the MD simulations, with Nosé–Hoover thermostat and barostat. In all the simulations, the timestep is 10^{-15} s.

The calculations have been performed on computer clusters (Intel® 8-core Xeon® X5365 or Intel® Core™2 Quad Q8200 4-core processors, OS Linux SUSE 10 SLES or 11, Intel® MPI 3.0 or MPICH 1.2.7 parallel computing libraries) in St. Petersburg State University.

3. Results and discussion

3.1. Pure silver iodide

At the preliminary stage of the work, to simulate the bulk phase of pure AgI, a MD cell has been constructed containing $12 \times 12 \times 12 = 1728$ α-AgI elementary cells, that is, 3456 Ag ions and 3456 I ions. Initially,

Table 1
PRV and ShK parameter sets for AgI.

	PRV	ShK		PRV	ShK
q_{Ag} ($\|e\|$)	0.6	0.5815	H_{II} (eV·Å^7)	6427.1	5325.2
q_I ($\|e\|$)	−0.6	−0.5815	P_{AgAg} (eV·Å^4)	0	0
n_{AgAg}	11	11	P_{AgI} (eV·Å^4)	16.888	14.898
n_{AgI}	9	9	P_{II} (eV·Å^4)	33.776	29.796
n_{II}	7	7	W_{AgAg} (eV·Å^6)	0	0
H_{AgAg} (eV·Å^{11})	0.21303	0.16235	W_{AgI}, (eV·Å^6)	0	0
H_{AgI} (eV·Å^9)	1647.4	1307.2	W_{II} (eV·Å^6)	99.767	84.41

Table 2
Calculated densities and diffusion coefficients of silver ions for the bulk α-AgI.

T (K)	PRV parameter set		ShK parameter set	
	ρ (g cm^{-3})	D_{Ag} (cm^2 s^{-1})	ρ (g cm^{-3})	D_{Ag} (cm^2 s^{-1})
500	5.63	$1.24 \cdot 10^{-5}$	5.99	$1.35 \cdot 10^{-5}$
600	5.49	$2.1 \cdot 10^{-5}$	5.85	$2.3 \cdot 10^{-5}$
700	5.35	$3.2 \cdot 10^{-5}$	5.69	$3.5 \cdot 10^{-5}$
800	5.21	$4.5 \cdot 10^{-5}$	5.54	$4.7 \cdot 10^{-5}$
900	5.08	$5.8 \cdot 10^{-5}$	5.38	$6.2 \cdot 10^{-5}$
1000	4.94	$7.4 \cdot 10^{-5}$	5.21	$7.9 \cdot 10^{-5}$

iodine ions are placed in the sites of a bcc lattice, and silver ions, in randomly chosen b or d positions according to Polyakov [25]. Standard periodic boundary conditions (PBC) are imposed on the system. The electrostatic energy is calculated using Ewald summation. MD trajectories up to 800 ps in length are generated for temperatures 500, 600, 700, 800, 900, and 1000 K, and zero pressure.

Both potential parameter sets used (PRV and ShK) allow to reproduce a phase that retains α-AgI structure over a MD trajectory ~100 ps length. The ShK set gives densities close to the experimental ones for α-phase, while those calculated for the PRV set are ~10% lower; silver ions are 5–10% more mobile in the ShK model (Table 2).

It is difficult to convert the model system to the molten state due to the PBC imposed. To achieve that, the system has been thermostated at 2000 K for 50 ps, then cooled again to 1000 K. The diffusion coefficient of iodine ions in the melt was ~$2 \cdot 10^{-5}$ cm^2/s for both parameter sets.

On the whole, ShK parameters give densities, silver ion diffusion coefficients, and ion–ion pair distribution functions for α-AgI close to those calculated in [22].

At the same time, for both PRV and ShK sets, in longer MD runs (400–600 ps) we have observed in the model system a transition to a state with ~20% higher density and structural characteristics that can be understood as suggesting a rocksalt-like structure being formed: the coordination numbers in the first coordination sphere are $N_{I-I} \approx 12$, $N_{Ag-I} \approx 6$, while α-phase has $N_{I-I} \approx 14$, $N_{Ag-I} \approx 4$. As it is mentioned above, experiment detects such a transition only at high pressures (~3000 atm at 370 K, ~7000 atm at 500 K) [11].

The disagreement between these results and the conclusions made in previous simulations of AgI [22,26], that the Parrinello–Rahman–Vashishta model allows to reproduce both α and β phases of AgI as stable at zero pressure (although the pressure of $\alpha \rightarrow$ rocksalt transition estimated in [26] is lower than the experimental one), can be explained by the fact that those authors worked with much smaller MD cells (the largest, in [22], contained 250 Ag ions and 250 I ions).

We have concluded that the simple Parrinello–Rahman–Vashishta model with ShK parameters can be used as a first approximation for simulations of AgI, particularly AgI-containing nanosystems. At the same time, it is likely that an improvement of the model potential is desirable for a better account of co-operative effects that determine, to a great extent, relative stability of different crystal structures.

In the further simulations, the ShK parameter set is used.

3.2. Filling of carbon SWNTs by AgI and structure of AgI INTs

After equilibrating model silver iodide melt at 1000 K, a hole is created in the center of the MD cell by removing an equal number of Ag and I ions, and a carbon SWNT is placed in the hole. Then, the system is thermostated and barostated at 500 K and zero pressure for 300 ps. During the MD run, the SWNT is filled by AgI, and at the same time, the melt freezes. We perform the procedure for carbon nanotubes with different chiral vectors: (9,8), (9,9), (10,7), (10,8), (10,9), (10,10), (11,8), (11,9), (11,10), (11,11), and (12,8), 25 Å and 40 Å in length.

After the filling, a carbon SWNT with AgI inside can be taken out from the melt by removing all Ag and I ions outside the SWNT (observing the condition of electroneutrality of the system). So, we get a nanotube or nanowire of silver iodide in a tube. The AgI nanostructures having been formed in the 40 Å tubes are "multiplied" 5 times, and the 5 copies placed in an isolated carbon SWNT, 200 Å in length. Then, the system (AgI in a long isolated carbon SWNT) is equilibrated for 300–500 ps at 1200 K, and cooled to 500 K and equilibrated again for 900 ps. This method of generating model AgI

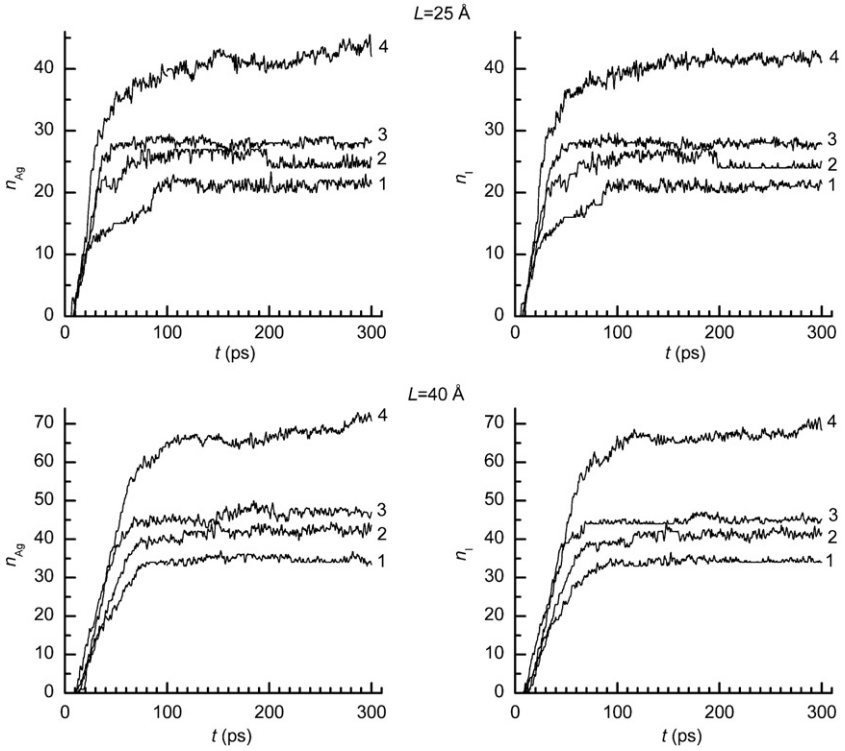

Fig. 1. Time dependence of the number of Ag (left) and I (right) ions inside carbon SWNTs during the process of filling: 1 — (9,8) carbon nanotube; 2 — (9,9); 3 — (11,8); 4 — (11,11).

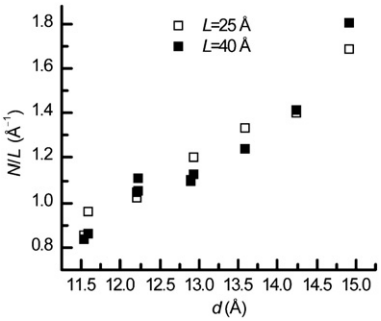

Fig. 2. The mean number of AgI formula units (per 1 Å of a nanotube length) inside filled carbon SWNTs of different diameters.

structures in 200 Å SWNTs is used, because such a long tube does not fit into the MD cell used when the bulk AgI is simulated with PBC.

Fig. 1 shows the time dependence of the number of silver and iodine ions in carbon nanotubes being filled. The filling time is within 100 ps for all tubes except perhaps the widest ones, (11,11). *N*/*L*, the mean number of AgI formula units within a carbon SWNT after equilibration, per unit length of the nanotube, is presented as a function of the SWNT's diameter in Fig. 2. The *N*/*L* values are, within statistical error limits, quite close to those reported in [7] for a simple idealized (Born–Mayer) potential.

After a filled carbon SWNT is equilibrated at 500 K, we examine the geometry of the AgI@SWNT structure. These structures can be seen as consisting of Ag–I chains, and for all the tubes except (11,11), the chains form, basically, a single-wall AgI nanotube that can be considered either as a slightly distorted (due to thermal motion) cylinder produced from a square-net or hexagonal plane by folding it with a certain chiral vector [8], or as a combination of fragments of this type with different chiral vectors. In (11,11) carbon SWNTs, there is an additional Ag–I chain, with some I–Ag–I–Ag squares inserted in it, near the tube axis, while all other Ag and I ions form the "outer" INT similar to single-wall AgI tubes in narrower carbon SWNTs. A shifted upward *N*/*L* value for (11,11) tubes (Fig. 2) is obviously a result of the structural change in AgI@SWNT.

The geometries (morphologies) of AgI INTs formed in carbon SWNTs (in the (11,11) case, of the "outer" INT), characterized by chiral vectors, are listed in Table 3, using the same notation as in [8]. Fig. 3 shows some of these structures.

While the AgI INT geometry is obviously dependent on the diameter of the carbon SWNT being filled, varying the chiral vector with the diameter kept approximately constant has no distinct effect on the INT structure. There are cases when two INT morphologies coexist in one tube for some time, and then an evolution occurs that leads to a configuration characterized by one single INT chiral vector, as in (11,9) and (11,10) carbon SWNTs. During such a "restructuring", the drift of average configurational energy is no more than 1 kJ/mol, while a typical difference between energies of two INTs with different

Table 3
AgI INT geometry in carbon SWNTs. (*n*,*m*) is the chiral vector of carbon SWNT, *d* is the tube diameter, and *L*, its length. The "+" sign means combination of fragments of two INT structures. The "→" sign means evolution of such a combination in a long MD run (2.5 ns).

d (Å)	(*n*,*m*)	*L* (Å)		
		25	40	200
11.52	(9,8)	$(2,2)_{hex}$	$(2,2)_{hex}$	$(2,2)_{hex}$
11.57	(10,7)	$(3,3)_{sq}$	$(2,2)_{hex}$	$(2,2)_{hex}$
12.19	(9,9)	$(3,3)_{sq}$	$(3,3)_{sq}$	$(3,2)_{hex}+(3,3)_{sq}$
12.21	(10,8)	$(3,2)_{hex}$	$(3,3)_{sq}$	$(3,3)_{sq}$
12.87	(10,9)	$(3,2)_{hex}$	$(3,2)_{hex}$	$(3,2)_{hex}$
12.92	(11,8)	$(4,3)_{sq}$	$(4,0)_{hex}$	$(3,2)_{hex}$
13.54	(10,10)	$(3,3)_{hex}$	$(4,1)_{hex}$	$(3,3)_{hex}$
13.56	(11,9)	$(3,3)_{hex}$	$(4,1)_{hex}$	$(4,1)_{hex}+(3,3)_{hex}\rightarrow(4,1)_{hex}$
13.63	(12,8)	$(3,3)_{hex}$	$(3,3)_{hex}$	$(3,3)_{hex}$
14.22	(11,10)	$(4,3)_{hex}$	$(3,3)_{hex}$	$(3,3)_{hex}+(4,2)_{hex}\rightarrow(3,3)_{hex}$
14.90	(11,11)	$(4,3)_{hex}$	$(4,3)_{hex}$	$(6,0)_{hex}+(5,1)_{hex}\rightarrow(6,0)_{hex}$

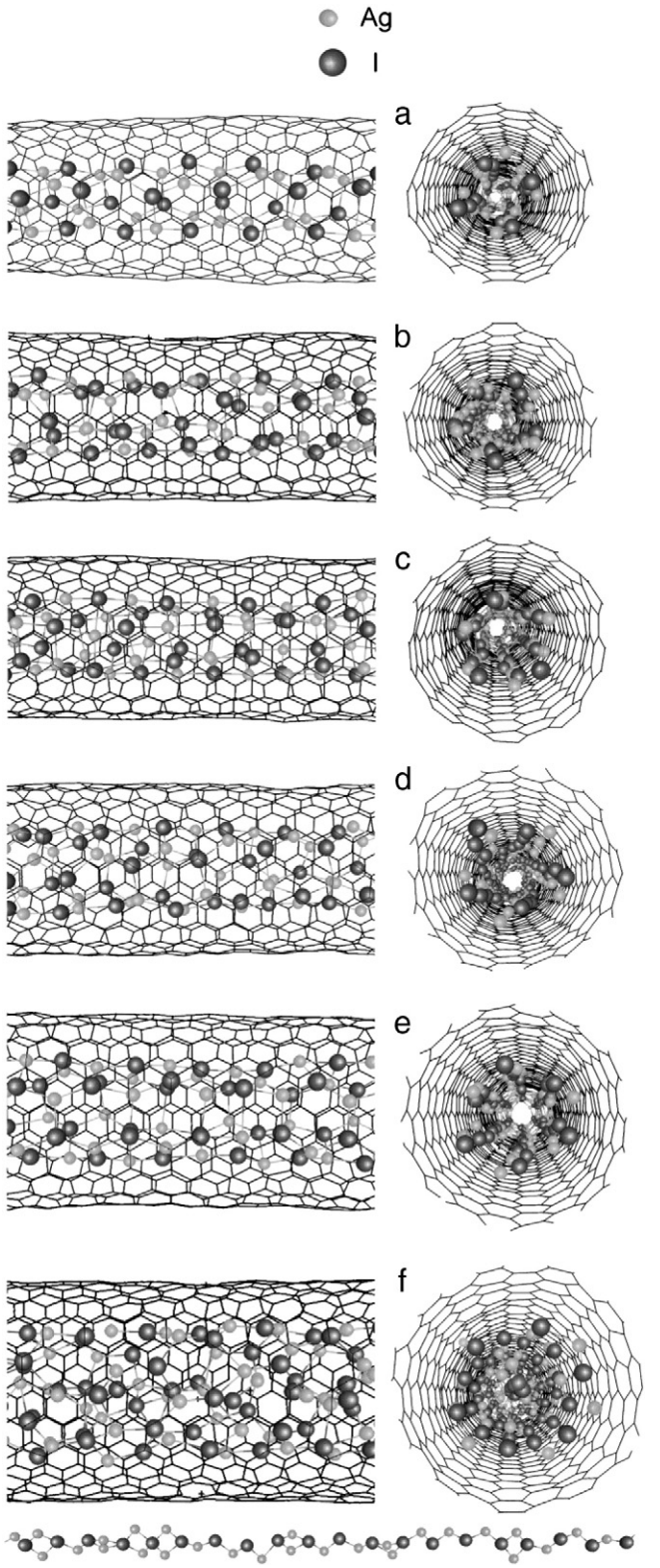

Fig. 3. Typical AgI@SWNT structures in filled carbon nanotubes (200 Å in length) at 500 K, side and sectional front view: (a) (9,8) carbon SWNT, $(2,2)_{hex}$ AgI INT; (b) (9,9) carbon SWNT, $(3,2)_{hex}$ AgI INT fragment; (c) (9,9) carbon SWNT, $(3,3)_{sq}$ AgI INT fragment; (d) (10,9) carbon SWNT, $(3,2)_{hex}$ AgI INT; (e) (10,10) carbon SWNT, $(3,3)_{hex}$ AgI INT; (f) (11,11) carbon SWNT, $(6,0)_{hex}$ AgI INT fragment (distorted), the additional AgI chain that goes along the tube axis is also shown separately.

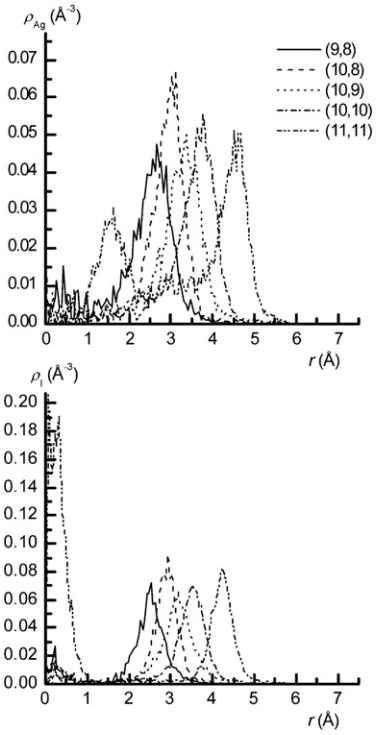

Fig. 4. Density profiles for silver (top) and iodine (bottom) ions, $\rho_{Ag}(r)$ and $\rho_I(r)$ (r is the distance from the tube axis) in carbon SWNTs at 500 K.

chiral vectors (morphologies), with diameters corresponding to the energetic minimum for the respective chiral vector, is significantly higher, according to calculations based on an idealized model potential chosen so as to predict a wurtzite-like ground-state crystal structure [10]. One can also see that for the model potential used in the present work, INT structures based on a folded hexagonal AgI plane are, in most cases, preferable to those based on a folded square-net plane. However, INTs of the latter class can also be produced (specifically, two AgI@(9,9)SWNT morphologies coexisting in one tube are shown in Fig. 3, b, c). This agrees with the simulation results for bulk AgI described above (implying that the ShK potential likely allows to reproduce not only hexagonal but also rocksalt-like phase of silver iodide), as well as with [19] where both hexagonal and square-like fragments were observed in simulated AgI@SWNT structures. At the same time, this leads to an INT "phase" (morphology) diagram as a function of carbon nanotube diameter different from the diagram obtained in [8] using a model potential chosen to reproduce a hexagonal structure with certainty. Particularly, in our case, unlike [8], there is a tube diameter range where $(3,3)_{sq}$ AgI INT is stable (between the width intervals with preference for $(2,2)_{hex}$ and $(3,2)_{hex}$ INTs).

Fig. 4 presents silver and iodine ions density profiles in some of the simulated carbon SWNTs. They illustrate the increase of AgI INT width with the carbon SWNT diameter. Indeed, in all carbon SWNTs, I ion density $\rho_I(r)$ has maximum at r values 3.18–3.32 Å lower than the carbon tube radius. The corresponding maximum of the density $\rho_{Ag}(r)$ of Ag ions (smaller and more mobile than iodine) is 0.1–0.25 Å closer to the carbon tube wall. In the (11,11) carbon SWNT, unlike all others,

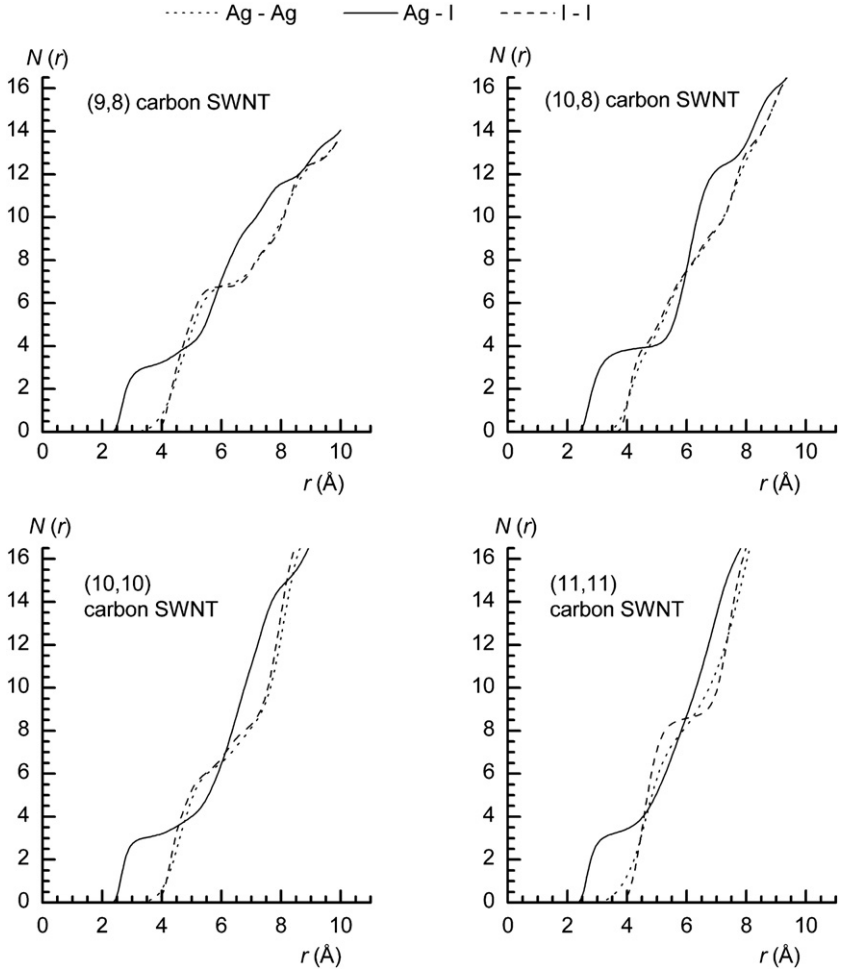

Fig. 5. The average number of neighbors within the distance r for Ag–Ag, Ag–I, I–I pairs of ions in carbon SWNTs at 500 K.

second peaks appear on the density profiles, with iodine ions concentrated near the tube axis and silver ions distributed in a layer between the axis and the "outer" INT. In narrower tubes, the ion densities near the axis are much lower than near the maxima but still clearly different from zero, and significantly higher for silver ions than for iodine ones, that corresponds to defects in the INT structure and to weaker bonding (respectively, higher mobility) of Ag ions as compared to iodine ones, like in the bulk AgI.

Figs. 5 and 6 show Ag–Ag, Ag–I, and I–I coordination characteristics in some tubes: the average number $N(r)$ of ions of one type within the sphere of radius r around an ion of another type, and the radial distribution functions. From $N(r)$ plots, one can see that in the (10,8) carbon SWNT, the Ag–I first coordination number is close to 4 and not to 3 as in other tubes, that corresponds to the difference between tetragonal and hexagonal INT geometries.

The simulation results can be compared with data obtained from experimental studies of silver (or copper) halide nanocrystalline structures being formed in carbon SWNTs [1,27,28]. Particularly, we can compare the model $(3,3)_{hex}$ AgI INTs in (10,10) carbon tubes ($d = 13.54$ Å for an "ideal" tube) with the structure of silver iodide in carbon SWNTs with $d = (13.4 \pm 0.5)$ Å obtained from HRTEM in [28]. The first peaks of I–I and Ag–I radial distribution functions at 500 K calculated by MD correspond to the distances $r_{1(I-I)} \approx 4.3$ Å and $r_{1(Ag-I)} \approx 2.65$ Å, respectively, while the results reported in [28] suggest that the former value should be about 4.6 Å at room temperature, and for the bulk hexagonal phase of silver iodide (β-AgI), EXAFS measurements give $r_{1(I-I)} \approx 4.59$ Å and $r_{1(Ag-I)} \approx 2.81$ Å [29]. This can be interpreted as a slight underestimation of the effective radius of iodine ion in the model used in the simulations, that agrees with the above-mentioned fact that the simulated system shows a stronger tendency to form a rocksalt-like bulk structure in comparison with the experimental data for AgI. Both the MD simulations and the experiment [28] give an AgI INT structure in the tube that can be viewed as a stack of $(AgI)_3$ units, with iodine ions forming triangles whose orientation alternates along the tube axis (ABABAB… packing), and silver ions mostly tetrahedrically coordinated, having three iodine ions and one carbon atom in the first coordination shell, with some lateral contraction of the tetrahedra due to the presence of carbon SWNT. However, while the experimental data suggest that the AgI structure in the tube is a fragment of β-AgI bulk crystal (wurtzite structure), the simulated silver iodide in carbon SWNTs tends to form "classical" hexagonal nanotubes. The latter result agrees with the simulations by Wootton and Harrowell [18] who studied model AgI nanoclusters at zero temperature in vacuum, not confined by a carbon tube. This difference between simulations and experiment confirms the desirability of a certain improvement of the model potential for AgI. At the same time, the suggestion made in [18], that nanotube- or fullerene-like AgI clusters also may be experimentally observable, is likely to deserve a further check.

3.3. Ion diffusion in AgI INTs in carbon SWNTs

The ion mobility is investigated in long (~200 Å) nanotubes. MD trajectories 4–8 ns in length are generated. From ion mean square

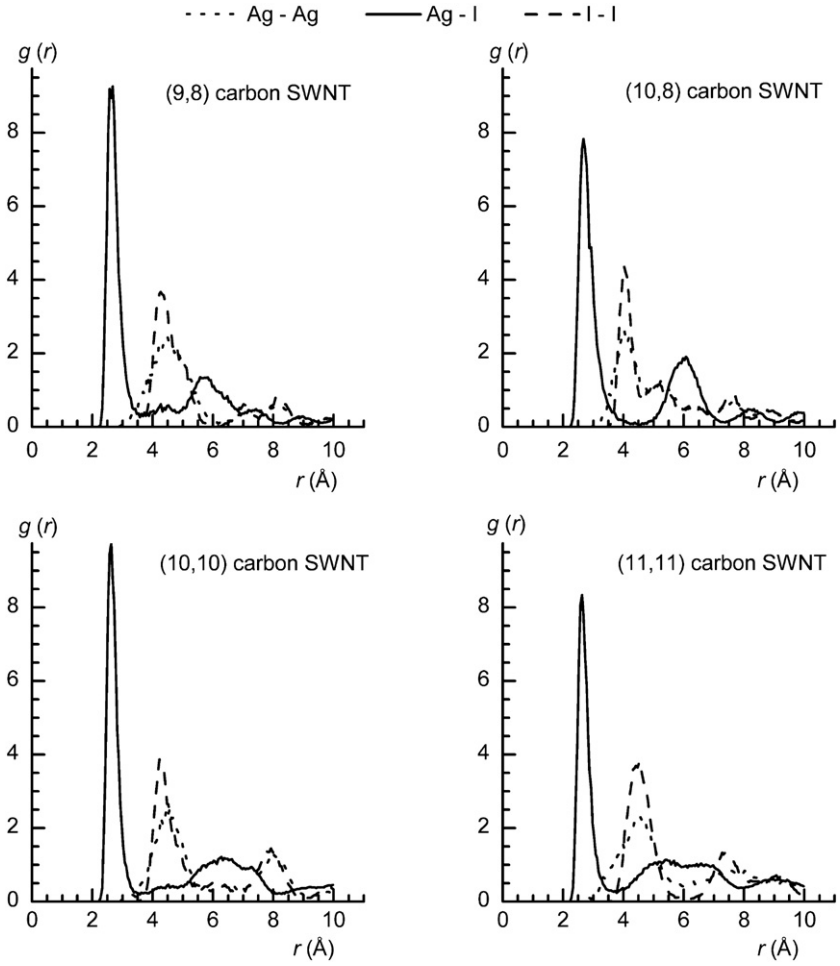

Fig. 6. Ag–Ag, Ag–I, I–I radial distribution functions in carbon SWNTs at 500 K.

displacements, the diffusion coefficients are calculated. As we are interested only in ion migration along the tube axis, the version of Einstein equation used is

$$\left\langle \Delta z^2 \right\rangle = 2Dt \tag{4}$$

where D is the diffusion coefficient, and Δz is ion displacement along the direction of the tube axis. The formula can be used when $|\Delta z|$ is significantly less than the tube length.

The calculated diffusion coefficients are presented in Fig. 7. On the whole, the ion mobility, both of silver and iodine, in narrow carbon SWNTs is lower and diffusion activation energy is higher than in the bulk phase of AgI.

Ion mobility is the lowest in the (10,8) carbon SWNT where a $(3,3)_{sq}$ AgI INT is formed, and the second lowest, in the (9,9) tube where fragments of $(3,3)_{sq}$ and $(3,2)_{hex}$ silver iodide INTs coexist. In the (10,8) carbon nanotube, the diffusion of silver ions becomes detectable only at 1000 K, and of iodines, at 1200 K. The activation energy of Ag diffusion is ~0.85 eV in (10,8) tube (the highest value of all the tubes examined) and ~0.6 eV in (9,9) tube. The high stability of $(3,3)_{sq}$ structure agrees with the results of AgI nanoclusters simulation [18] suggesting that in a small system, such a structure ("flattened wurtzite", or "hexagonal stacks") can have lower energy than β-AgI ("wurtzite") fragments due to higher coordination of the edge ions.

Both narrower carbon SWNTs with $(2,2)_{hex}$ AgI INTs and wider ones with $(3,2)_{hex}$ AgI INTs are characterized by higher diffusion coefficients of silver ions D_{Ag}. In $(2,2)_{hex}$ AgI nanotubes in (9,8) and (10,7) carbon SWNTs, D_{Ag} values are quite close, with the activation energy ~0.45 eV. The difference in D_{Ag} between AgI@SWNT systems on the base of (10,9) and (11,8) carbon tubes ($(3,2)_{hex}$ AgI INTs) is significantly higher; the calculated activation energy is ~0.46 eV in (10,9) carbon SWNT (slightly narrower and with lower ion mobility) and ~0.42 eV in (11,8) tube.

For still wider (10,10), (11,9), and (12,8) carbon SWNTs (diameter from 13.54 Å to 13.63 Å), where $(3,3)_{hex}$ or $(4,1)_{hex}$ silver iodide INTs are formed, the simulation gives, again, very close D_{Ag} values. The activation energy is 0.53–0.57 eV, higher than in tubes with $(3,2)_{hex}$ AgI INTs. Similar to the case of $(3,3)_{sq}$ morphology, this agrees with molecular mechanics calculations [18] showing that fragments of $(3,3)_{hex}$ nanotubes are also among the lowest-energy AgI clusters.

In the (11,10) carbon nanotube, where $(3,3)_{hex}$ silver iodide INT is formed with larger free space in the tube, the mobility of both Ag and I ions increases significantly in comparison with narrower tubes with $(3,3)_{hex}$ AgI structure inside.

Finally, (11,11) carbon SWNT, the widest among those examined, shows the best silver ion diffusion, that becomes visible already at

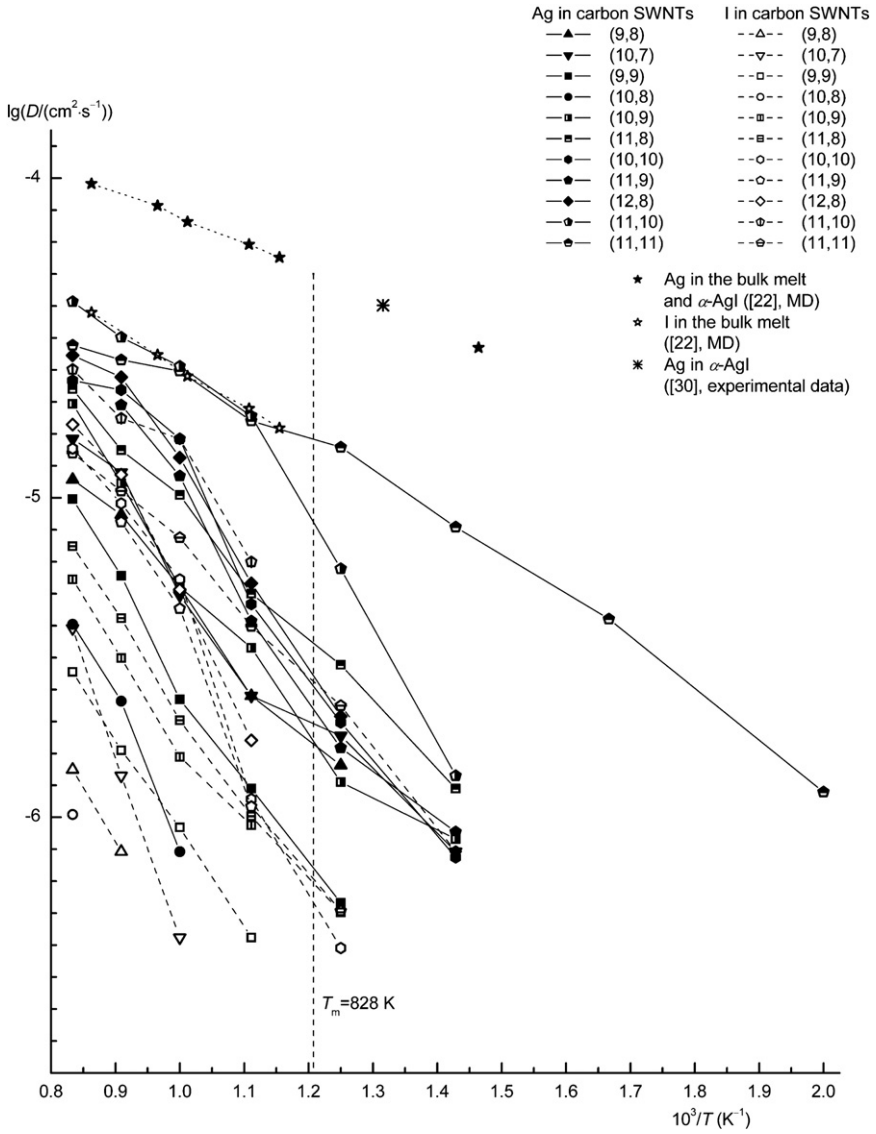

Fig. 7. Diffusion coefficients of silver and iodine ions in simulated AgI@SWNT. The data for bulk AgI [22,30] are also given. T_m is the experimental melting point of AgI.

500–600 K, with activation energy about 0.28 eV in the 500–800 K temperature range and about 0.17 eV in the 800–1200 K range. The latter value is very close to the activation energy calculated for the bulk AgI melt in [22], although the absolute values of D_{Ag} in the nanotube are 2.5–3 times lower than in the bulk. For larger I ions, the activation energy in the tube is still higher than in the bulk melt (~0.38 eV and ~0.23 eV, respectively). The change is obviously due to the fact that in the (11,11) carbon SWNT, not a single-wall AgI INT is formed but a structure with a significant number of Ag and I ions near the tube axis where the environment of silver ions is more similar to the Ag-conducting bulk phase.

At $T \geq 1000$ K, AgI melts in the nanotubes, having an effect of increased iodine diffusion and lowered silver diffusion activation energy.

At lower temperatures, an interval can be determined where AgI@SWNT shows a significant Ag ion mobility while iodine positions are mostly fixed and thus a stable structure is maintained. In the (11,11) carbon SWNT, such a "superionic" AgI@SWNT state exists at 500–600 K, and in the carbon tubes with diameter between 12.8 Å and 13.7 Å (with $(3,2)_{hex}$, $(4,1)_{hex}$ and $(3,3)_{hex}$ AgI INTs), at 700–800 K. This is a much narrower temperature range that for the bulk α-AgI superionic polymorph. However, the model gives evidence that it is, in principle, possible to produce AgI fast-conducting nanotube structures, specifically in carbon SWNTs.

Typical Ag ion trajectories, with thermal oscillation noise eliminated by smoothing, in two of the simulated AgI@SWNT systems are presented in Fig. 8. The temperatures are in the range where AgI in the tube shows well visible silver ion diffusion but no appreciable migration of iodines. The "smoothed out" Ag diffusive motion is close to a standard pattern of jumps between lattice sites in ionic crystals with high concentration of defects, especially for simpler morphologies like $(2,2)_{hex}$ AgI INT in a (9,8) carbon SWNT. At the same time, examining the system configurations along the MD trajectory without coordinate

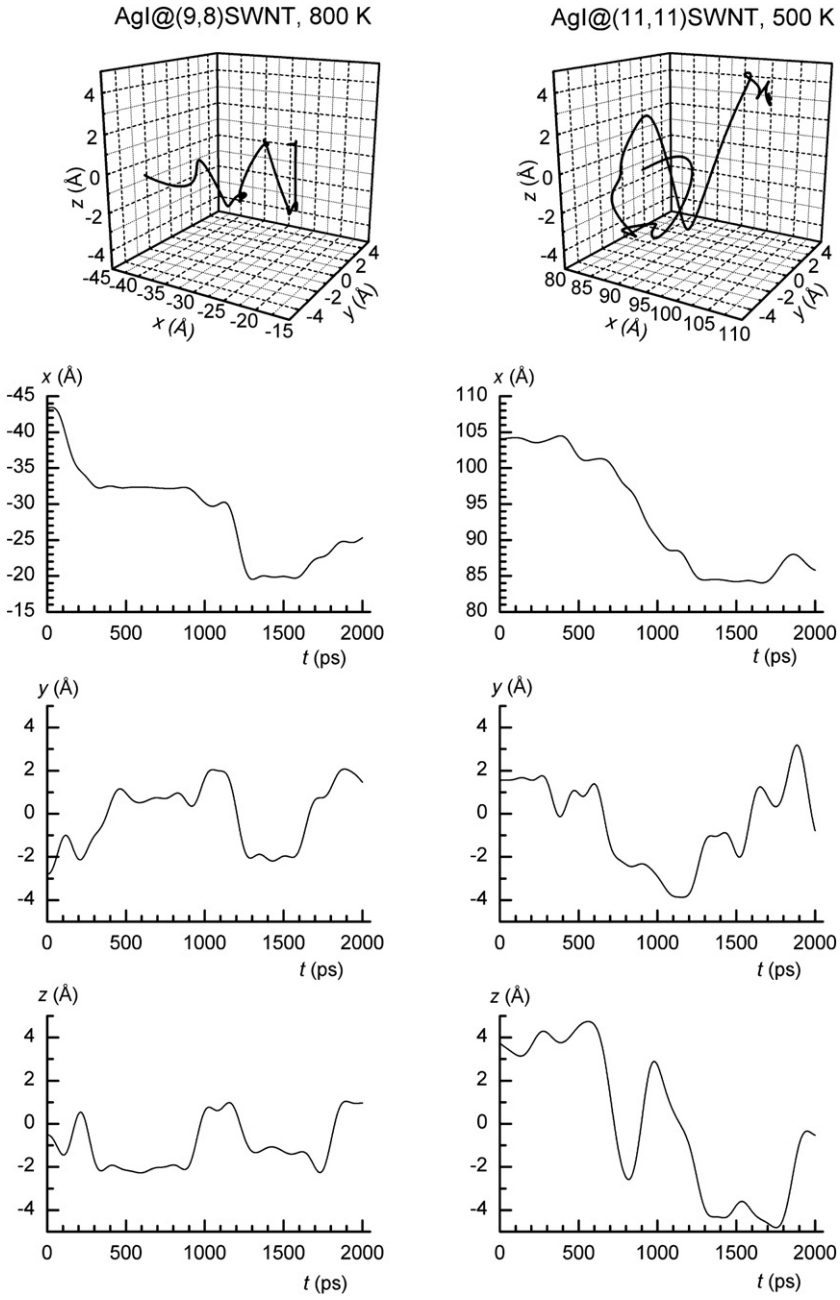

Fig. 8. Typical (smoothed) Ag ion trajectories in AgI@SWNT at temperatures of significant silver, bur not iodine, ion mobility: a three-dimensional trajectory and smoothed time dependence of coordinates. The tubes are oriented along the *x* axis.

smoothing reveals a highly cooperative nature of the ion motion, with significant local perturbations of the structure. Together with high diffusion activation energies, this is quite similar to the premelting behavior of bulk silver bromide observed in MD simulations earlier; such a behavior can perhaps be interpreted as a first stage of the superionic transition, interrupted by crystal melting [31]. The difference between AgI@SWNT INTs and bulk AgI that, according to the experimental data, has a distinct first-order transition from the β-phase to the superionic α-polymorph, can be explained by higher rigidity of the silver iodide INT structures, less favorable to Ag ion walking in the "free space" left between ions in the iodine sublattice. It can be noted here that 7–9 nm γ-AgI particles (with sphalerite, i.e. cubic diamond-like, structure) also were experimentally shown to differ from β-AgI in having not a first-order but a rather diffuse second-order transition to the high-conducting state [32].

4. Conclusions

The MD computer simulation has allowed to reproduce AgI INT formation in carbon SWNTs. Examining their structural characteristics in different carbon tubes shows that silver iodide, where the anion radius is significantly higher than in AgCl or AgBr, can form nanocrystalline tubular structures both with trigonal ion coordination and with tetragonal one, with preferences depending on the tube geometry. In most cases, trigonal structures are produced, but a stable "hexagonal stacks" $(3,3)_{sq}$ structure, with tetragonal coordination, is detected in some tubes. It must be noted, however, that the model potential used may overestimate, to some degree, the energetic advantage of tetragonal structures (i.e. effectively underestimates the iodine anion radius).

A transition to a "silver-conducting" state is observed on heating the AgI INTs in carbon SWNTs before melting. In such a state, a diffusive motion of Ag ions occurs against the background of relatively stable average iodine positions (no appreciable increase of iodine mean square displacement with time) but with significant local perturbations of the crystal structure. This may be similar to premelting reproduced earlier in simulations of bulk AgBr (that, contrary to AgI, has no experimentally observed phase transition to a superionic state). So, in the simulated AgI@SWNT nanostructures, the silver ion mobility increase on heating is accompanied not by full-scale structural changes but rather by strong local cooperative perturbations, unlike in the thermodynamically stable bulk phase of AgI. Further, more detailed studies can clarify the nature of the high-conducting solid state of silver halide nanotubes.

Acknowledgement

The work has been supported by the Russian Foundation for Basic Research (project No 08.03.01039).

References

[1] J. Sloan, A.L. Kirkland, J.L. Hutchison, M.L.H. Green, Chem. Commun. 13 (2002) 1319.
[2] J. Sloan, M. Terrones, S. Nufer, S. Friedrichs, S.R. Bailey, H.-G. Woo, M. Rühle, J.L. Hutchison, M.L.H. Green, J. Am. Chem. Soc. 124 (2002) 2116.
[3] M.V. Kharlamova, M.V. Chernysheva, A.A. Eliseyev, "Rusnanotech'08" Nanotechnology International Forum, Moscow, 2008, p. 414.
[4] M. Wilson, P.A. Madden, J. Am. Chem. Soc. 123 (2001) 2101.
[5] M. Wilson, Nano Lett. 4 (2004) 299.
[6] M. Wilson, S. Friedrichs, Acta Cryst. A 62 (2006) 287.
[7] M. Wilson, J. Chem. Phys. 124 (2006) 124706.
[8] M. Wilson, Faraday Discuss. 134 (2007) 283.
[9] C.L. Bishop, M. Wilson, J. Phys. Condens. Matter 21 (2009) 115301.
[10] M. Wilson, J. Chem. Phys. 131 (2009) 214507.
[11] B.-E. Mellander, Phys. Rev. B 26 (1982) 5886.
[12] S. Ono, M. Kobayashi, S. Kashida, T. Ohachi, Solid State Ionics 178 (2007) 1023.
[13] L.-F. Liu, S.-W. Lee, J.-B. Li, M. Alexe, G.-H. Rao, W.-Y. Zhou, J.-J. Lee, W. Lee, U. Gösele, Nanotechnology 19 (2008) 495706.
[14] A.K. Ivanov-Shitz, Crystallogr. Rep. 52 (2007) 302.
[15] S. Matsunaga, Solid State Ionics 176 (2005) 1929.
[16] S. Matsunaga, J. Non-Cryst. Solids 353 (2007) 3459.
[17] V. Bitrián, J. Trullàs, J. Phys. Chem. B 112 (2008) 1718.
[18] A. Wootton, P. Harrowell, J. Phys. Chem. B 108 (2004) 8412.
[19] M. Baldoni, S. Leoni, A. Sgamelotti, G. Seifert, F. Mercuri, Small 3 (2007) 1730.
[20] J.S. Bendall, A. Ilie, M.E. Welland, J. Sloan, M.L.H. Green, J. Phys. Chem. B 110 (2006) 6569.
[21] M. Parrinello, A. Rahman, P. Vashishta, Phys. Rev. Lett. 50 (1983) 1073.
[22] F. Shimojo, M. Kobayashi, J. Phys. Soc. Jpn 60 (1991) 3725.
[23] J. Tersoff, Phys. Rev. B 39 (1989) 5566.
[24] W. Smith, The DL_POLY molecular simulation package, http://www.cse.clrc.ac.uk/msi/software/DL_POLY/.
[25] V.I. Polyakov, Crystallogr. Rep. 46 (2001) 435.
[26] J.L. Tallon, Phys. Rev. B 38 (1988) 9069.
[27] N.A. Kiselev, R.M. Zakalyukin, O.M. Zhigalina, N. Grobert, A.S. Kumskov, Yu.V. Grigoriev, M.V. Chernysheva, A.A. Eliseev, A.V. Krestinin, Yu.D. Tretyakov, B. Freitag, J.L. Hutchison, J. Microsc. 232 (2008) 335.
[28] A.A. Eliseev, L.V. Yashina, M.M. Brzhezinskaya, M.V. Chernysheva, M.V. Kharlamova, N.I. Verbitsky, A.V. Lukashin, N.A. Kiselev, A.S. Kumskov, R.M. Zakalyukin, J.L. Hutchison, B. Freitag, A.S. Vinogradov, Carbon 48 (2010) 2708.
[29] G. Dalba, P. Fornasini, S. Mobilio, F. Rocca, Philos. Mag. B 59 (1989) 143.
[30] A. Kvist, R. Taerneberg, Z. Naturforsch. A 25 (1970) 257.
[31] A.K. Ivanov-Schitz, G.N. Mazo, E.S. Povolotskaya, S.N. Savvin, Solid State Ionics 173 (2004) 103.
[32] Y. Wang, L. Huang, H. He, M. Li, Phys. B 325 (2003) 357.